Stem Cell Research 29 (2018) 189–196

Contents lists available at ScienceDirect

Stem Cell Research

journal homepage: www.elsevier.com/locate/scr

Direct conversion of human pluripotent stem cells into cranial motor neurons using a piggyBac vector

Riccardo De Santis[a,b], Maria Giovanna Garone[b], Francesca Pagani[a], Valeria de Turris[a], Silvia Di Angelantonio[a,c], Alessandro Rosa[a,b,*]

[a] Center for Life Nano Science, Istituto Italiano di Tecnologia, Viale Regina Elena 291, 00161 Rome, Italy
[b] Department of Biology and Biotechnology Charles Darwin, Sapienza University of Rome, P.le A. Moro 5, 00185 Rome, Italy
[c] Department of Physiology and Pharmacology, Sapienza University of Rome, P.le A. Moro 5, 00185 Rome, Italy

ARTICLE INFO

Keywords:
Spinal motor neuron
Cranial motor neuron
Induced pluripotent stem cells
Amyotrophic lateral sclerosis
Phox2a
piggyBac

ABSTRACT

Human pluripotent stem cells (PSCs) are widely used for in vitro disease modeling. One of the challenges in the field is represented by the ability of converting human PSCs into specific disease-relevant cell types. The nervous system is composed of a wide variety of neuronal types with selective vulnerability in neurodegenerative diseases. This is particularly relevant for motor neuron diseases, in which different motor neurons populations show a different susceptibility to degeneration. Here we developed a fast and efficient method to convert human induced Pluripotent Stem Cells into cranial motor neurons of the branchiomotor and visceral motor subtype. These populations represent the motor neuron subgroup that is primarily affected by a severe form of amyotrophic lateral sclerosis with bulbar onset and worst prognosis. This goal was achieved by stable integration of an inducible vector, based on the piggyBac transposon, allowing controlled activation of Ngn2, Isl1 and Phox2a (NIP). The NIP module effectively produced electrophysiologically active cranial motor neurons. Our method can be easily extended to PSCs carrying disease-associated mutations, thus providing a useful tool to shed light on the cellular and molecular bases of selective motor neuron vulnerability in pathological conditions.

1. Introduction

Pluripotent stem cells (PSCs) are widely used to model in vitro neurodegenerative diseases, which usually affect specific subtypes of neurons. Both human Embryonic Stem Cells (ESCs) and induced Pluripotent Stem Cells (iPSCs) can be converted into disease relevant cell types, included neurons, thus providing a cell system to study the molecular and cellular mechanisms underlying neurodegeneration. The possibility of deriving patient-specific iPSCs and the recent advent of genome editing techniques further expand the potential of such systems, allowing the production of human neurons carrying disease-associated mutations. PSCs-derived mutant neurons can also provide a platform to screen for drugs. To fully exploit the potential of PSCs in the field of neurodegeneration, appropriate protocols for producing pure populations of specific neuronal subtypes are needed. To this aim, a significant effort has been put on the development and optimization of methods to obtain, for instance, cortical (Suzuki and Vanderhaeghen, 2015), dopaminergic (Arenas et al., 2015), hippocampal (Yu et al., 2014) or motor (Davis-Dusenbery et al., 2014) neurons.

Motor neurons represent the primary cell type affected in a number of diseases that are collectively referred to as motor neuron diseases, and include Amyotrophic Lateral Sclerosis (ALS) and Spinal Muscular Atrophy (SMA). The developmental program of motor neurons has been well decoded (Jessell, 2000). Two main motoneurons subtypes are present in the central nervous system in human. Spinal motor neurons are located in the ventral spinal cord and innervate body skeletal muscles (Price and Briscoe, 2004). Cranial motor neurons reside in the brainstem (midbrain and hindbrain) and comprise three subsets: branchiomotor (BM), visceral motor (VM) and somatic motor (SM) (Guthrie, 2007). BM axons innervate muscles controlling the jaw, facial expression, pharynx and larynx. VM neurons control salivary and lacrimal glands, smooth muscle and visceral organs. SM neurons innervate eye (oculomotor, trochlear and abducens) and tongue (hypoglossal) muscles. Not all MN subtypes are equally vulnerable in ALS and SMA. Despite pathogenic proteins are ubiquitously expressed, in most ALS patients MNs controlling eye movements are generally spared, MNs innervating pelvic floor muscles are relatively resistant to degeneration and faster spinal motor units are affected before slower ones (Nijssen et al., 2017). Differential vulnerability of specific MN subgroups seems to be due to intrinsic factors, as protective effects were

* Corresponding author at: Department of Biology and Biotechnology Charles Darwin, Sapienza University of Rome, P.le A. Moro 5, 00185 Rome, Italy.
E-mail address: alessandro.rosa@uniroma1.it (A. Rosa).

https://doi.org/10.1016/j.scr.2018.04.012
Received 31 December 2017; Received in revised form 23 March 2018; Accepted 24 April 2018
Available online 27 April 2018

observed upon overexpression of oculomotor-enriched factors or reduction of spinal MNs-enriched factors (Allodi et al., 2016; Kaplan et al., 2014).

ALS prognosis depends from the site of onset of the first symptoms (Wijesekera and Leigh, 2009). Spinal onset ALS is the most frequent, with symptoms starting in upper and lower limbs, and is usually fatal at 3–5 years post-diagnosis. Conversely, speech and swallowing problems are noticed first in a more severe form of ALS (bulbar onset), with limb symptoms arising almost simultaneously. Bulbar onset ALS has the worst prognosis, with an average survival of 2–3 years. The incidence of spinal or bulbar onset is not uniformly distributed in patients carrying different mutations associated to familial ALS (FALS). For instance, the percentage of bulbar onset is significantly higher in patients with FUS or TARDBP mutations than that of patients with SOD1 mutations (Yan et al., 2010).

Taken together, the different susceptibility of specific MNs subtypes to neurodegeneration and the onset of symptoms in different motor units seem due to intrinsic factors. Human PSCs represent a promising system to shed light on these mechanisms, provided that appropriate protocols are established to convert them into specific MN subtypes. In this work, we present a method to differentiate human pluripotent stem cells into cranial MNs. Existing differentiation protocols are generally designed to generate spinal MNs as they rely on the activity of retinoic acid (RA), which during embryonic development confer a posterior character to neural progenitors (Boulting et al., 2011; Amoroso et al., 2013; Maury et al., 2015). Here we developed an inducible system that allows fast and efficient generation of cranial MNs with a BM and VM character, in extremely simplified culture conditions.

2. Material and methods

2.1. Plasmid construction and generation of a stable human iPSC line

The epB-Bsd-TT-NIL and epB-Bsd-TT-NIP plasmids were generated by inserting the sequences of, respectively, Ngn2-F2A-Isl1-T2A-Lhx3 (NIL) and Ngn2-F2A-Isl1-T2A-Phox2a (NIP) in the enhanced piggyBac transposable vector epB-Bsd-TT (Rosa et al., 2014). NIL and NIP were obtained from the iNIL and iNIP constructs described in (Mazzoni et al., 2013) and cloned between the *Bam*HI and *Not*I sites of epB-Bsd-TT. The resulting constructs contain the enhanced piggyBac terminal repeats flanking a constitutive cassette driving the expression of the Blasticidin resistance gene fused to the rtTA gene and, in the opposite direction, a tetracycline-responsive promoter element (TRE) driving the expression of NIP or NIL. Human iPSCs used in this study belong to the lines WT I (main figures) and FUS-P525L/P525L (Fig. S1) described in (Lenzi et al., 2015). iPSCs were co-transfected with 4.5 μg of transposable vector and 0.5 μg of the piggyBac transposase using the Neon Transfection System (Life Technologies) as previously described (Lenzi et al., 2015). Selection in 5 μg/ml blasticidin gave rise to stable and inducible cell lines.

2.2. Cranial and spinal MN differentiation

iPSCs, maintained as previously described (Lenzi et al., 2015), were dissociated to single cells with Accutase (Thermo Fisher Scientific) and plated in Nutristem-XF/FF medium (Biological Industries) supplemented with 10 μM rock inhibitor (Enzo Life Sciences) on Matrigel (BD Biosciences) at a density of 100′000 cells/cm^2. The day after differentiation was induced by adding 1 μg/ml doxycycline (dox) (Thermo Fisher Scientific) in Nutristem without bFGF and TGFβ (Biological Industries). Similar results were obtained when DMEM/F12 (Sigma Aldrich) was used instead of Nutristem without bFGF and TGFβ. Medium was changed every day. After 48 h of dox induction, medium was changed to Neurobasal/B27 medium (Neurobasal Medium, Thermo Fisher Scientific, supplemented with 1X B27, Thermo Fisher Scientific, 1X Glutamax, Thermo Fisher Scientific, 1X NEAA, Thermo Fisher Scientific, and 0.5X Penicillin/Streptomycin, Sigma Aldrich), containing 5 μM DAPT and 4 μM SU5402 (both from Sigma Aldrich). At day 5, cells were dissociated with Accutase (Thermo Fisher Scientific) and plated on poly-ornithine/laminin (Sigma Aldrich) or alternatively on Matrigel (BD Biosciences) coated dishes or 12 well removable chamber slides or 8 well chamber slides (Ibidi) at the density of 100′000 cells per cm^2. 10 μM rock inhibitor was added for the first 24 h after dissociation. Neuronal cultures were maintained in neuronal medium (Neurobasal/B27 medium supplemented with 20 ng/ml BDNF, 10 ng/ml GDNF, both from PreproTech, and 200 ng/ml L-ascorbic acid, Sigma Aldrich).

2.3. RNA analysis

Total RNA was extracted with the Quick RNA MiniPrep (Zymo Research) and retrotranscribed with PrimeScript RT reagent Kit (Perfect Real Time). Targets were analyzed by real-time qRT-PCR with SYBR Green Power-UP (Thermo Fisher Scientific). The internal control used was the housekeeping gene *ATP5O*. Primers sequences are reported in Table S1.

2.4. Immunostaining

Cells were fixed with 4% PFA for 15 min at room temperature. Immunostaining was performed with anti-Islet-1/2 (1:50, 39.4D5; DSHB), anti-TUJ1 (1:1000; T2200; Sigma-Aldrich), anti-Phox2b (B-11) (1:50; sc-376,997; Santa Cruz Biotechnology), anti-CHAT (1:100; ab144P; Abcam) primary antibodies and anti-mouse Alexa Fluor 488 (1:200, Thermo Fisher Scientific), anti-rabbit Alexa Fluor 594 (1:200, Immunological Sciences) and anti-goat Alexa Fluor 594 (1:200, Immunological Sciences) donkey secondary antibodies. Fluorescent images were acquired at the Olympus iX83 FluoView1200 laser scanning confocal microscope using a UPLSAPO10x2, NA 0,40 air objective. Standard setting for DAPI, Alexa 488 and Alexa 594 were used. Images on Fig. 1C were acquired with 2× zoom, 1600 × 1600 pixel. Images on Fig. 3 were acquired with 3× zoom, 1024 × 1024 pixel. Automated cell counting was performed with the Cell Scoring tool of MetaMorph software (Molecular Devices).

2.5. Patch-clamp recordings

Whole-cell patch-clamp recordings were used for the functional characterization of iPSC-derived cranial MNs, plated on Matrigel. Experiments were performed in a recording chamber continuously perfused with an external solution containing (in mM): 140 NaCl, 2.8 KCl, $CaCl_2$, 2 $MgCl_2$, 10 HEPES, 10 glucose (pH 7.3 with NaOH; 300 mOsm) at room temperature. Borosilicate pipettes were filled with a solution containing (in mM): 140 K-gluconate, 2 NaCl, 5 BAPTA, 2 MgCl2, 10 HEPES, 2 Mg-ATP, 0.3 Na-GTP (pH 7.3 with KOH; 290 mOsm). Cells were visualized with a BX51WI microscope (Olympus). Voltage- and current- clamp recordings were performed using Axon DigiData 1550 (Molecular Devices). Signals were filtered at 2 KHz, digitized (10 kHz) and collected using Clampex 10 (Molecular Devices). Whole-cell capacitance (Cm), cell membrane resistance (Rm) and Resting Membrane Potential (RMP) were measured on line by Clampex. Cells were clamped at −70 mV to measure spontaneous activity. An on-line P4 leak subtraction protocol was used for all recordings of voltage-activated currents. Voltage steps (50 ms duration) from −100 to +40 mV (10 mV increment; holding potential −60 mV) were applied to study voltage-activated sodium currents. Voltage-activated potassium currents were evoked by voltage steps (250 ms duration) from −30 to +50 mV (10 mV increment, holding potential −40 mV). Firing properties of iPSC-derived cranial MNs were investigated in current-clamp mode, injecting current pulses (1 s duration) of increasing amplitude (from 20 to 80 pA; 20 pA increment), after imposing a membrane potential of −60 mV to each cell (injection of −14.6 ± 2.1 pA). Data were analyzed off-line with Clampfit 10 and

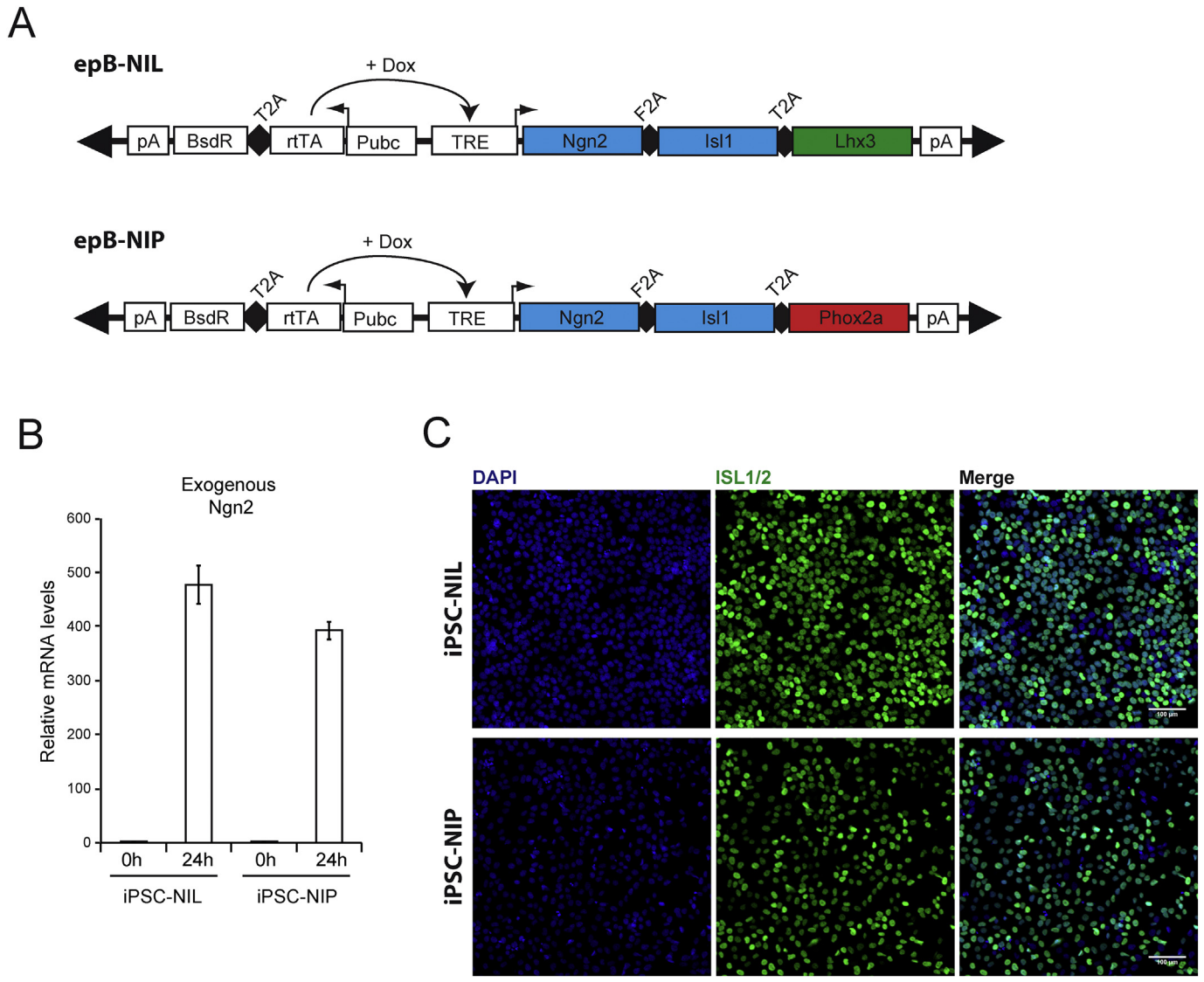

Fig. 1. Generation of iPSC-NIL and iPSC-NIP cells.
(A) Schematic representation of the epB-NIL and epB-NIP constructs. pA: polyadenylation signal; BsdR: blasticidin resistance gene; T2A: self-cleavage peptide; rtTA: TET transactivator protein gene; Pubc: human Ubiquitin C constitutive promoter; TRE: TET responsive element; Dox: doxycycline. Black triangles represent terminal repeats of the transposon. (B) iPSC-NIL and iPSC-NIP cells were collected before (0 h) or after (24 h) 24 h of doxycycline treatment and the expression of Ngn2 was analyzed by real-time qRT-PCR with primers specific for the exogenous Ngn2. (C) Immunostaining analysis of Isl1/2 protein (green) in iPSC-NIL and iPSC-NIP cells treated with doxycycline for 24 h. Nuclei were counterstained with DAPI (blue). Scalebar for all panels: 100 μm. (For interpretation of the references to colour in this figure legend, the reader is referred to the web version of this article.)

Origin 7 software.

3. Results and discussion

3.1. Generation of stable and inducible iPSC lines

Motor neuron identity in the brainstem is specified by the diffusible action of FGF8 and retinoic acid (RA), which set the expression of Hox genes along the rostrocaudal axis. Dorsoventral patterning is instead determined by a gradient of Sonic hedgehog (SHH), diffusing dorsally from the floor plate and the notochord, which sets two distinct progenitor domains: p3, containing progenitors of BM and VM neurons that express *Nkx2.2* and *Nkx2.9*; and pMN, containing progenitors of SM neurons that express *Pax6* and *Olig2*. Postmitotic BM and VM neurons in the hindbrain are characterized by the expression of Islet-1, Phox2b, Phox2a and Tbx20, while SM neurons express Hb9, Lhx3 and Lhx4 (Guthrie, 2007). In mouse embryonic stem cells, ectopic expression of Ngn2, Isl1 and Lhx3 (NIL) induces a spinal MN identity, while Ngn2 and Isl1 plus Phox2a (NIP) specify cranial MNs (Mazzoni et al., 2013). NIL ectopic expression has been shown to induce a spinal MN fate in human PSCs as well (Hester et al., 2011; Goto et al., 2017). However, to the best of our knowledge, the NIP module has never been used in human.

We have previously shown that MyoD expression from an "enhanced" piggyBac vector (epB) can efficiently convert human iPSCs into skeletal muscle (Lenzi et al., 2016). Replacement of the MyoD coding sequence with the NIL or NIP module led to the generation of epB-NIL and epB-NIP vectors, respectively (Fig. 1A). These vectors allow the coordinated expression of the three factors upon doxycycline exposure. Human iPSCs were co-transfected with the piggyBac transposase and either epB-NIL or epB-NIP, generating stable and inducible lines (hereafter iPSC-NIL and iPSC-NIP). To test the inducible expression from the constructs, iPSC-NIL and iPSC-NIP cells were treated with doxycycline for 24 h. As shown in Fig. 1B, we observed a strong induction of the exogenous Ngn2 transcript in both lines. We then assayed

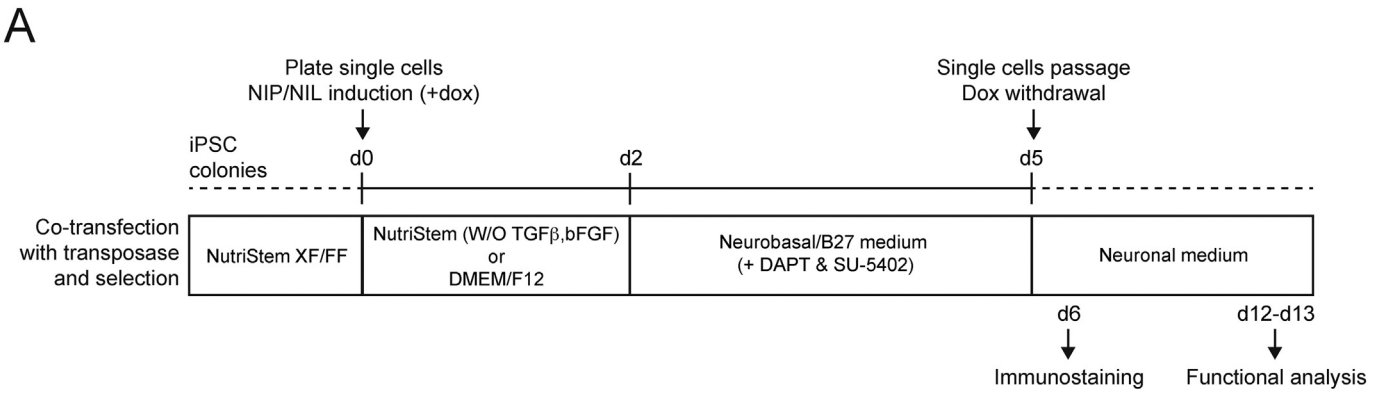

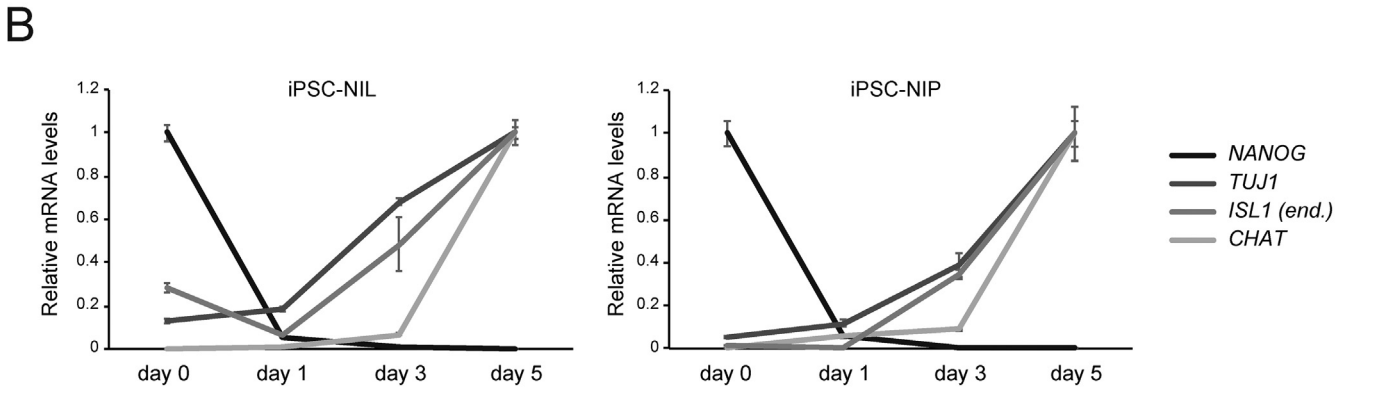

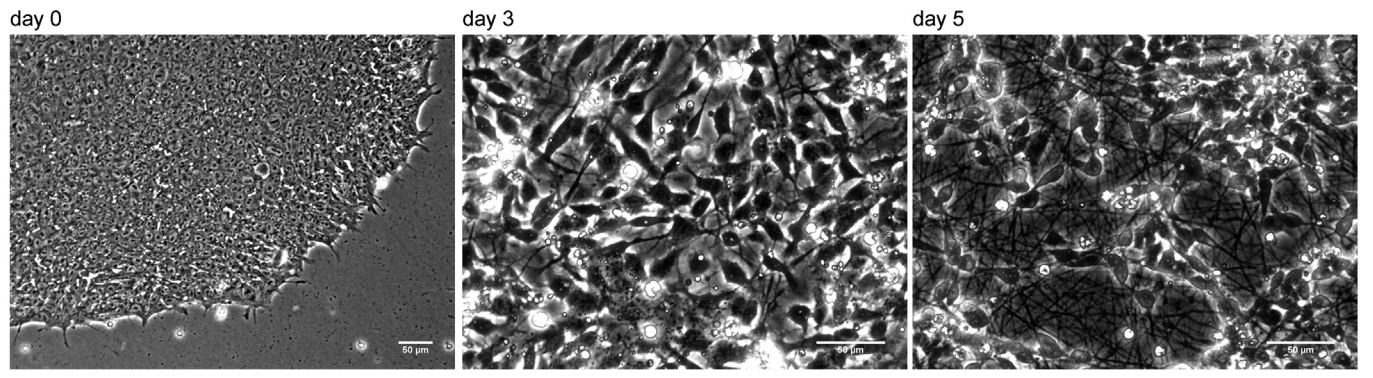

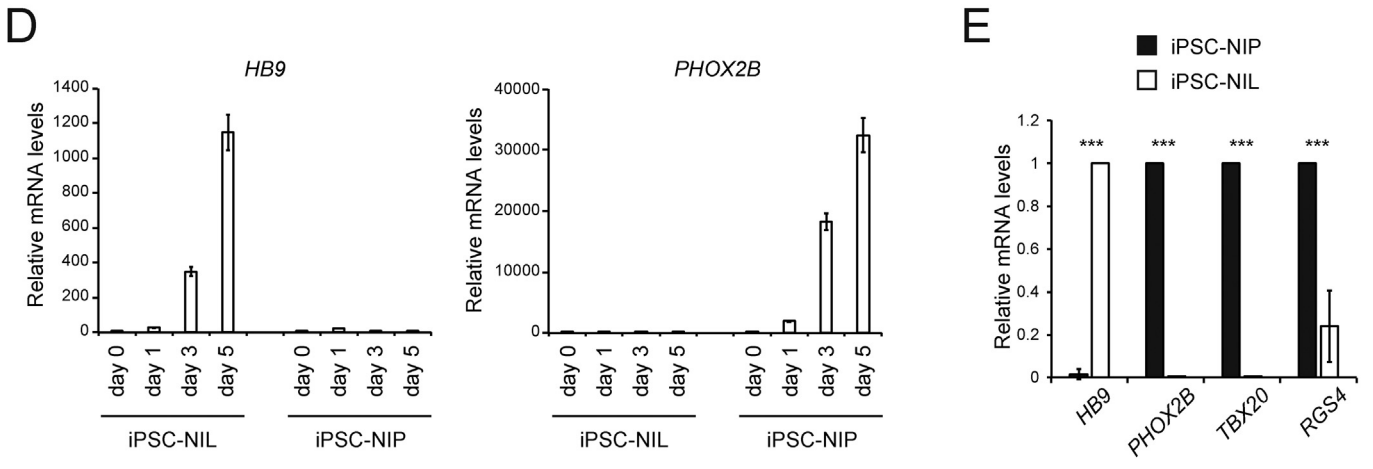

(caption on next page)

Fig. 2. MN differentiation.
(A) Schematic representation of the differentiation protocol. Dox: doxycycline. (B) Analysis of the expression of the indicated markers in differentiating iPSC-NIL (left) or iPSC-NIP (right) cells by real-time qRT-PCR. For each marker the time point with the highest expression has been used as the calibrator sample. Primers used for *ISL1* are specific for the endogenous gene. (C) Brightfield images of differentiating iPSC-NIP at the indicated time points. Scale bar for all panels: 50 µm. (D) Analysis of the expression of *HB9* (left) and *PHOX2B* (right) in differentiating iPSC-NIL and iPSC-NIP cells by real-time qRT-PCR. Day 0 has been used as the calibrator sample. (E) Comparative analysis by real-time qRT-PCR of the expression of MN markers after 5 days of differentiation of iPSC-NIL and iPSC-NIP cells. Histogram bars represent the average of 3 independent experiments and error bars indicate the standard deviation (Student's *t*-test; paired; two tails; *** = $p < 0.001$).

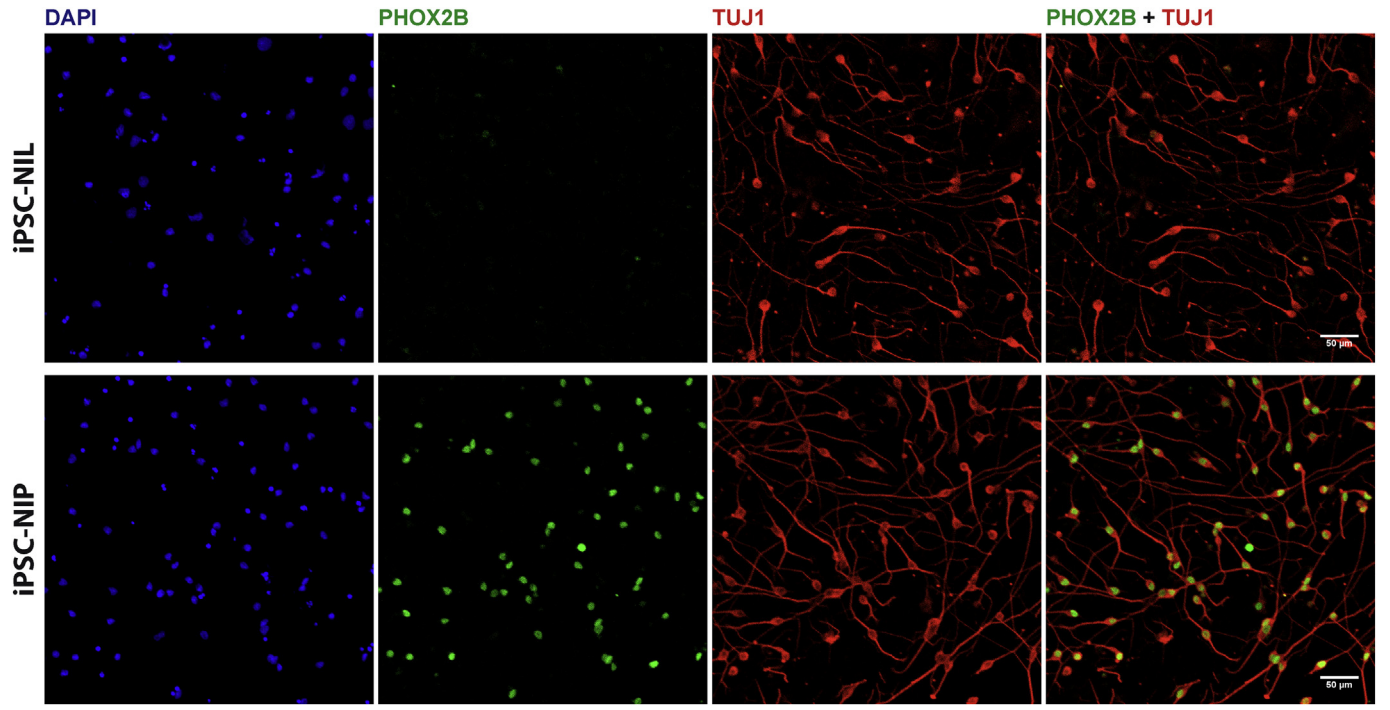

Fig. 3. Immunostaining analysis of NIP-induced MNs.
Immunostaining for the cranial MN marker PHOX2B (green) and the pan-neuronal marker TUJ1 (red) in iPSC-NIL and iPSC-NIP cells differentiated as shown in Fig. 2A, dissociated, re-plated on poly-L-ornithine laminin-coated chambered slides and maintained in neural medium for 24 h. Nuclei are counterstained with DAPI. Scale bar for all panels: 50 µm. (For interpretation of the references to colour in this figure legend, the reader is referred to the web version of this article.)

by immunostaining the production of the transgenic Isl1 protein, which was detected in > 80% of cell nuclei of doxycycline-treated iPSC-NIL and iPSC-NIP cells (Fig. 1C).

3.2. Fast conversion of iPSC-NIP into cranial MNs

We designed a fast and simple protocol for cranial MN differentiation from iPSC-NIP and, in parallel, iPSC-NIL used as a control for spinal MN specification. The protocol is outlined in Fig. 2A. NIL and NIP expression was induced by doxycycline in a medium devoid of bFGF and TGF-beta agonists. After 48 h, the medium was switched, for additional 3 days, to a neural medium containing the γ-secretase inhibitor DAPT and the FGF antagonist SU5402. The combined activity of these two molecules was previously shown to accelerate post-mitotic MNs specification (Maury et al., 2015; De Santis et al., 2017).

Expression of specific markers was analyzed during the course of differentiation (Fig. 2B). By day 1, both iPSC-NIL and iPSC-NIP cells had rapidly downregulated the pluripotency gene *NANOG*. At day 3 we observed an increase of the pan-neuronal marker *TUBB3* (*TUJ1*), which further increased at day 5. Similarly, both cell lines gradually acquired the expression of the MN gene *ISL1*. Expression of the choline acetyltransferase (*CHAT*), a characteristic feature of cholinergic neurons and late MN marker, was slightly induced at day 3 and strongly upregulated at day 5. Changes in gene expression were paralleled by a change in morphology during the course of differentiation, with a gradual increase of neuron-like cells over time (Fig. 2C).

We then analyzed the expression of markers of specific MN subtypes. Notably, *HB9* expression was induced at day 3 and further increased at day 5 only in iPSC-NIL, while the cranial MN gene *PHOX2B* showed a similar pattern of expression only in iPSC-NIP (Fig. 2D). These results suggest that during the course of differentiation iPSC-NIL and iPSC-NIP acquire different and alternative MN identities. We further confirmed this observation by a comparative analysis of additional cranial MN markers in the two cell lines. As shown in Fig. 2E, *PHOX2B*, *TBX20* and *RGS4* were highly and significantly enriched in iPSC-NIP-derived neurons, in the absence of *HB9* expression.

Taken together, this pattern of gene expression suggests that Ngn2, Isl1 and Phox2a combined activity induces a cranial MN fate, with BM and VM subtypes character, in human iPSCs.

We further confirmed this conclusion by prolonging the culture of NIP-induced MNs beyond day 5. Cells were dissociated and re-seeded in the absence of doxycycline. Immunostaining analysis showed that both iPSC-NIL- and iPSC-NIP-derived neurons expressed the TUJ1 neurofilament, marking mostly post-mitotic neurons (Fig. 3). However, only iPSC-NIP-derived neurons were positive for the cranial MN marker PHOX2B. Efficiency of differentiation was assessed by automated cell counting, resulting in 90% TUJ1-positive cells, of which 95% where also PHOX2B positive (about 1500 counted cells). Similar results were obtained with a second human iPSC line, carrying an ALS mutation in the FUS gene (Lenzi et al., 2015), confirming the robustness of the differentiation method (Fig. S1).

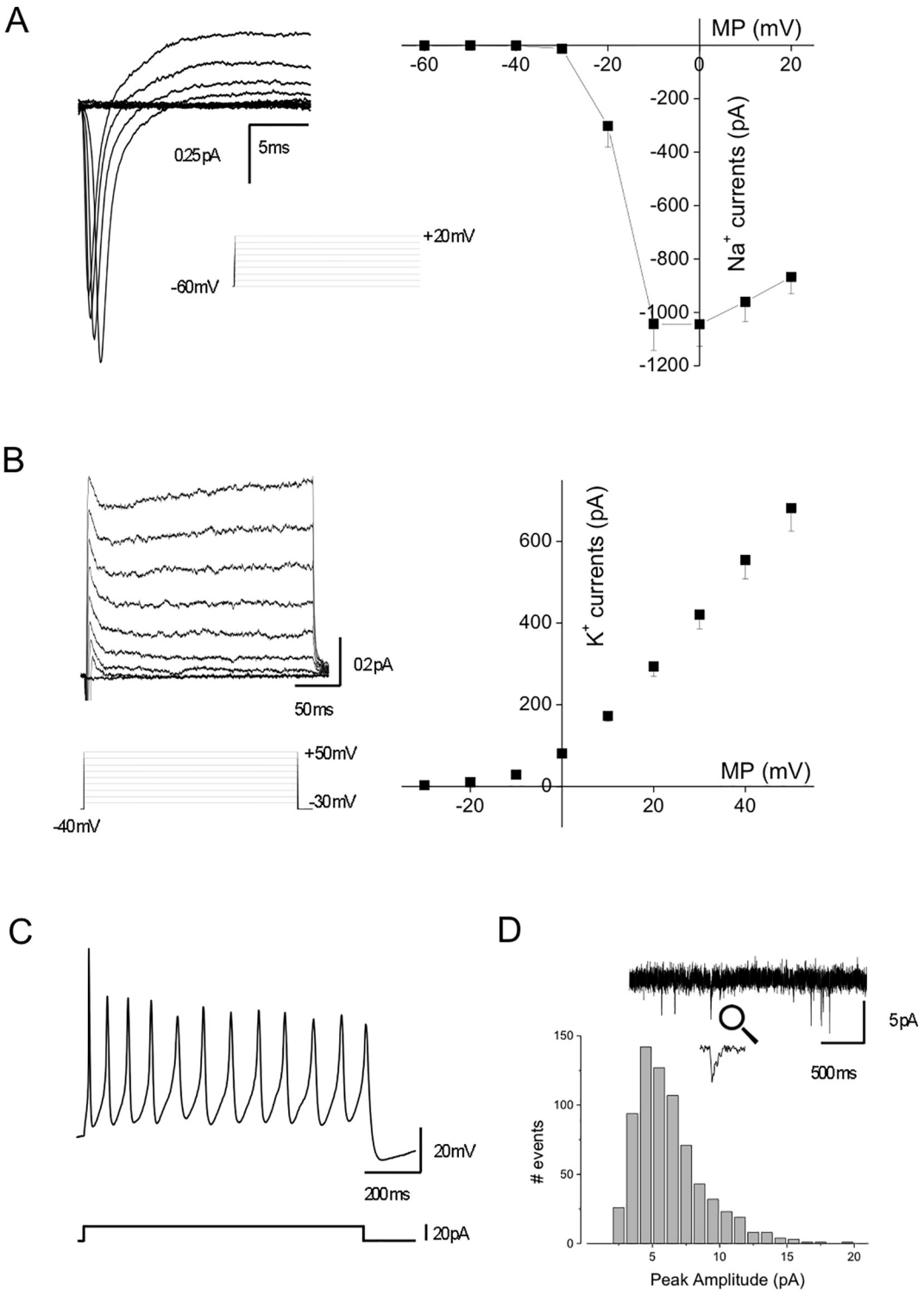

Fig. 4. Functional properties of iPSC-NIP-derived cranial MNs.
(A) Left: representative traces of voltage-dependent Na^+ currents recorded in an iPSC-NIP-derived cranial MN, in response to the stimulation protocol reported; right: mean voltage-current relationship of voltage-dependent Na^+ currents (n = 33, HP = −60 mV). (B) Left: representative recording of voltage-dependent K^+ currents evoked in a iPSC-NIP-derived cranial MN by the voltage steps reported; right: mean voltage-current relationship of voltage-dependent K^+ currents (n = 34; HP = −40 mV). (C) Current clamp recording of membrane voltage in response to current injection (20 pA, 1 s) in an iPSC-NIP-derived cranial MN showing a repetitive firing. (D) Histogram representing the distribution of peak amplitude (pA) of spontaneous glutamatergic events in iPSC-NIP-derived cranial MN culture recorded at HP = −70 mV (n = 6). Insert: sample trace of recorded spontaneous synaptic activity.

3.3. Functional analysis

We next assessed the degree of maturation achieved by iPSC-NIP-derived cranial MNs by assessing their functional properties. To investigate the expression of the passive electrophysiological properties, patch clamp recordings were performed on iPSC-NIP differentiated as in Fig. 2A, dissociated, re-plated on Matrigel and maintained for additional 7–8 days. At this time point, differentiated cells were

consistently CHAT-positive (Fig. S2). Resting membrane potential (−42.4 ± 1.5 mV; n = 36) and cell capacitance (20.1 ± 0.9 pF; n = 36) were similar to those previously reported for human iPSC-derived MNs (Devlin et al., 2015), while membrane resistance values were typical of immature cells (1342 ± 109 MΩ; n = 36; Miles et al., 2004). We then characterized the ability of MNs to generate trains of action potentials, fundamental to allow muscle contraction. iPSC-NIP-derived neurons display large inward voltage-dependent Na^+ currents (1044 ± 82 pA at 0 mV; n = 33; Fig. 4A), activated near −30 mV and peaked at −10–0 mV, and voltage-dependent K^+ currents (421 ± 35 pA at +30 mV; n = 34; Fig. 4B). Current pulses were able to induce trains of action potentials in almost all tested cells. The mean threshold for first action potential generation was −24.2 ± 1.1 mV (n = 14; 20 pA of current injection). The minimum current required to elicit repetitive firing was 29.1 ± 2.9 pA and the firing frequency was 9.8 ± 1.1 Hz (n = 14; Fig. 4C). iPSC-NIP induced neurons in culture display the ability to form functional networks as revealed by the presence of synaptic events recorded in voltage clamp configuration. As expected we observed only glutamatergic activity, as using a K-gluconate based intracellular solution no synaptic events were detected when cells were voltage clamped at 0 mV. Conversely at HP = −70 mV spontaneous glutamatergic postsynaptic currents were present in 6 over 14 cells recorded. This spontaneous activity was characterized by a frequency of 2.0 ± 0.4 Hz (n = 6) and a peak amplitude of −6.3 ± 0.1 pA (n = 6; Fig. 4D).

Overall, functional data suggest that iPSC-NIP induced neurons acquire functional properties similar to those previously reported for PSC-derived MNs (Miles et al., 2004; Devlin et al., 2015).

4. Discussion

One of the major challenges in the use of PSCs for biomedical purposes is the ability to program their differentiation into cell populations that are as much as possible enriched in desired cell type. Differentiation protocols to obtain specific neuronal subtypes are often costly, time consuming and require cell purification. These issues are particularly relevant when iPSC-derived neurons are produced for -omic approaches, requiring high amounts of homogeneous cell populations. Our method allows to specify human iPSC differentiation into a disease relevant cell type, cranial VM and BM neurons. So far, cranial MNs have been derived from human PSCs by differentiation in presence of a combination of patterning molecules, such as Wnt, FGF, retinoic acid and Shh, which must be provided at very narrow specific concentrations (Maury et al., 2015). Moreover, it has been previously shown that lentiviral vectors-mediated ectopic expression of Phox2a or Phox2b increased the fraction of VM neurons obtained when hESCs are differentiated in presence of FGF8 and Shh (Mong et al., 2014). We show here that the combined activity of Phox2a, Ngn2 and Isl1 can quickly convert human iPSCs into cranial MNs with high efficiency and reproducibility, in absence of patterning molecules and without the need of viral infection. Stable integration mediated by the epB vector allowed overcoming the poor transfection efficiency in human iPSCs (Fig. S3), resulting in about 90% of PHOX2B-positive neurons, consistently, from two different lines. By demonstrating the efficacy of the NIP module in human, our work extends the previous finding that the NIL combination could convert human PSCs to spinal MNs (Hester et al., 2011; Goto et al., 2017). Notably, the degree of maturation achieved by iPSC-NIP-derived cranial MNs in 11–12 days is similar to that previously reported for MNs derived from iPSCs by conventional methods and further matured for 10 weeks in vitro (Devlin et al., 2015). Moreover, at this time point the vast majority of iPSC-NIP-derived cranial MNs were CHAT-positive and electrophysiological characterization showed their ability to fire a train of action potentials over time in vitro, reaching a maximum frequency that has been previously reported for MNs derived from human ESCs only after > 31 days (Takazawa et al., 2012), demonstrating functional maturation.

Several lines of iPSCs carrying MN diseases-associated mutations have been recently derived (Dimos et al., 2008; Chang et al., 2011; Bilican et al., 2012; Lenzi et al., 2015) Comparison of cranial versus spinal MNs derived from those human iPSC lines will allow to shed light into cell intrinsic determinants that underlie the different susceptibility to degeneration of specific MN subtypes.

Acknowledgments

We thank Dr. E. Mazzoni (New York University) for kindly providing the iNIL and iNIP constructs and Dr. G. Peruzzi (Center for Life Nano Science, Rome) for the FACS analysis of Fig. S3. We are grateful to members of the Center for Life Nano Science for helpful discussion. This work was partially supported by a grant from AriSLA (pilot grant 2016 “StressFUS”).

Conflict of interest

The authors declare no competing financial interests.

Author contributions

AR and RDS conceived the project. RDS and MGG produced the epB-NIP and epB-NIL constructs, set up the differentiation protocol and performed RNA and immunostaining analyses. FP and SDA performed functional analysis and analyzed the data. VdT acquired and analyzed microscopy images. AR coordinated the work and wrote the paper.

Appendix A. Supplementary data

Supplementary data to this article can be found online at https://doi.org/10.1016/j.scr.2018.04.012.

References

Allodi, I., Comley, L., Nichterwitz, S., Nizzardo, M., Simone, C., Benitez, J.A., Cao, M., Corti, S., Hedlund, E., 2016. Differential neuronal vulnerability identifies IGF-2 as a protective factor in ALS. Sci. Rep. 6, 25960. http://dx.doi.org/10.1038/srep25960.

Amoroso, M.W., Croft, G.F., Williams, D.J., O'Keeffe, S., Carrasco, M.A., Davis, A.R., Roybon, L., Oakley, D.H., Maniatis, T., Henderson, C.E., Wichterle, H., 2013. Accelerated high-yield generation of limb-innervating motor neurons from human stem cells. J. Neurosci. 33, 574–586. http://dx.doi.org/10.1523/JNEUROSCI.0906-12.2013.

Arenas, E., Denham, M., Villaescusa, J.C., 2015. How to make a midbrain dopaminergic neuron. Development 142, 1918–1936. http://dx.doi.org/10.1242/dev.097394.

Bilican, B., Serio, A., Barmada, S.J., Nishimura, A.L., Sullivan, G.J., Carrasco, M., Phatnani, H.P., Puddifoot, C.A., Story, D., Fletcher, J., Park, I.-H., Friedman, B.A., Daley, G.Q., Wyllie, D.J.A., Hardingham, G.E., Wilmut, I., Finkbeiner, S., Maniatis, T., Shaw, C.E., Chandran, S., 2012. Mutant induced pluripotent stem cell lines recapitulate aspects of TDP-43 proteinopathies and reveal cell-specific vulnerability. Proc. Natl. Acad. Sci. U. S. A. 109, 5803–5808. http://dx.doi.org/10.1073/pnas.1202922109.

Boulting, G.L., Kiskinis, E., Croft, G.F., Amoroso, M.W., Oakley, D.H., Wainger, B.J., Williams, D.J., Kahler, D.J., Yamaki, M., Davidow, L., Rodolfa, C.T., Dimos, J.T., Mikkilineni, S., MacDermott, A.B., Woolf, C.J., Henderson, C.E., Wichterle, H., Eggan, K., 2011. A functionally characterized test set of human induced pluripotent stem cells. Nat. Biotechnol. 29, 279–286. http://dx.doi.org/10.1038/nbt.1783.

Chang, T., Zheng, W., Tsark, W., Bates, S., Huang, H., Lin, R.-J., Yee, J.-K., 2011. Brief report: phenotypic rescue of induced pluripotent stem cell-derived motoneurons of a spinal muscular atrophy patient. Stem Cells 29, 2090–2093. http://dx.doi.org/10.1002/stem.749.

Davis-Dusenbery, B.N., Williams, L.A., Klim, J.R., Eggan, K., 2014. How to make spinal motor neurons. Development 141, 491–501. http://dx.doi.org/10.1242/dev.097410.

Devlin, A.-C., Burr, K., Borooah, S., Foster, J.D., Cleary, E.M., Geti, I., Vallier, L., Shaw, C.E., Chandran, S., Miles, G.B., 2015. Human iPSC-derived motoneurons harbouring TARDBP or C9ORF72 ALS mutations are dysfunctional despite maintaining viability. Nat. Commun. 6, 5999. http://dx.doi.org/10.1038/ncomms6999.

Dimos, J.T., Rodolfa, K.T., Niakan, K.K., Weisenthal, L.M., Mitsumoto, H., Chung, W., Croft, G.F., Saphier, G., Leibel, R., Goland, R., Wichterle, H., Henderson, C.E., Eggan, K., 2008. Induced pluripotent stem cells generated from patients with ALS can be differentiated into motor neurons. Science 321, 1218–1221. http://dx.doi.org/10.1126/science.1158799.

Goto, K., Imamura, K., Komatsu, K., Mitani, K., Aiba, K., Nakatsuji, N., Inoue, M., Kawata, A., Yamashita, H., Takahashi, R., Inoue, H., 2017. Simple derivation of spinal motor neurons from ESCs/iPSCs using Sendai virus vectors. Mol. Ther. Methods Clin. Dev. 4,

115–125. http://dx.doi.org/10.1016/j.omtm.2016.12.007.
Guthrie, S., 2007. Patterning and axon guidance of cranial motor neurons. Nat. Rev. Neurosci. 8, 859–871. http://dx.doi.org/10.1038/nrn2254.
Hester, M.E., Murtha, M.J., Song, S., Rao, M., Miranda, C.J., Meyer, K., Tian, J., Boulting, G., Schaffer, D.V., Zhu, M.X., Pfaff, S.L., Gage, F.H., Kaspar, B.K., 2011. Rapid and efficient generation of functional motor neurons from human pluripotent stem cells using gene delivered transcription factor codes. Mol. Ther. 19, 1905–1912. http://dx.doi.org/10.1038/mt.2011.135.
Jessell, T.M., 2000. Neuronal specification in the spinal cord: inductive signals and transcriptional codes. Nat. Rev. Genet. 1, 20–29. http://dx.doi.org/10.1038/35049541.
Kaplan, A., Spiller, K.J., Towne, C., Kanning, K.C., Choe, G.T., Geber, A., Akay, T., Aebischer, P., Henderson, C.E., 2014. Neuronal matrix metalloproteinase-9 is a determinant of selective neurodegeneration. Neuron 81, 333–348. http://dx.doi.org/10.1016/j.neuron.2013.12.009.
Lenzi, J., De Santis, R., de Turris, V., Morlando, M., Laneve, P., Calvo, A., Caliendo, V., Chiò, A., Rosa, A., Bozzoni, I., 2015. ALS mutant FUS proteins are recruited into stress granules in induced pluripotent stem cells (iPSCs) derived motoneurons. Dis. Model. Mech. 8, 755–766. http://dx.doi.org/10.1242/dmm.020099.
Lenzi, J., Pagani, F., De Santis, R., Limatola, C., Bozzoni, I., Di Angelantonio, S., Rosa, A., 2016. Differentiation of control and ALS mutant human iPSCs into functional skeletal muscle cells, a tool for the study of neuromuscolar diseases. Stem Cell Res. http://dx.doi.org/10.1016/j.scr.2016.06.003.
Maury, Y., Côme, J., Piskorowski, R.A., Salah-Mohellibi, N., Chevaleyre, V., Peschanski, M., Martinat, C., Nedelec, S., 2015. Combinatorial analysis of developmental cues efficiently converts human pluripotent stem cells into multiple neuronal subtypes. Nat. Biotechnol. 33, 89–96. http://dx.doi.org/10.1038/nbt.3049.
Mazzoni, E.O., Mahony, S., Closser, M., Morrison, C.A., Nedelec, S., Williams, D.J., An, D., Gifford, D.K., Wichterle, H., 2013. Synergistic binding of transcription factors to cell-specific enhancers programs motor neuron identity. Nat. Neurosci. 16, 1219–1227. http://dx.doi.org/10.1038/nn.3467.
Miles, G.B., Yohn, D.C., Wichterle, H., Jessell, T.M., Rafuse, V.F., Brownstone, R.M., 2004. Functional properties of Motoneurons derived from mouse embryonic stem cells. J. Neurosci. 24, 7848–7858. http://dx.doi.org/10.1523/JNEUROSCI.1972-04.2004.
Mong, J., Panman, L., Alekseenko, Z., Kee, N., Stanton, L.W., Ericson, J., Perlmann, T., 2014. Transcription factor-induced lineage programming of noradrenaline and motor neurons from embryonic stem cells. Stem Cells 32, 609–622. http://dx.doi.org/10.1002/stem.1585.
Nijssen, J., Comley, L.H., Hedlund, E., 2017. Motor neuron vulnerability and resistance in amyotrophic lateral sclerosis. Acta Neuropathol. 133, 863–885. http://dx.doi.org/10.1007/s00401-017-1708-8.
Price, S.R., Briscoe, J., 2004. The generation and diversification of spinal motor neurons: signals and responses. Mech. Dev. 121, 1103–1115. http://dx.doi.org/10.1016/j.mod.2004.04.019.
Rosa, A., Papaioannou, M.D., Krzyspiak, J.E., Brivanlou, A.H., 2014. miR-373 is regulated by TGFβ signaling and promotes mesendoderm differentiation in human embryonic stem cells. Dev. Biol. http://dx.doi.org/10.1016/j.ydbio.2014.03.020.
De Santis, R., Santini, L., Colantoni, A., Peruzzi, G., de Turris, V., Alfano, V., Bozzoni, I., Rosa, A., 2017. Stem Cell Rep. 1–33. http://dx.doi.org/10.1016/j.stemcr.2017.09.004.
Suzuki, I.K., Vanderhaeghen, P., 2015. Is this a brain which I see before me? Modeling human neural development with pluripotent stem cells. Development 142, 3138–3150. http://dx.doi.org/10.1242/dev.120568.
Takazawa, T., Croft, G.F., Amoroso, M.W., Studer, L., Wichterle, H., Macdermott, A.B., 2012. Maturation of spinal motor neurons derived from human embryonic stem cells. PLoS ONE 7 (7), e40154. http://dx.doi.org/10.1371/journal.pone.0040154.
Wijesekera, L.C., Leigh, P.N., 2009. Amyotrophic lateral sclerosis. Orphanet J. Rare Dis. 4, 3. http://dx.doi.org/10.1186/1750-1172-4-3.
Yan, J., Deng, H.X., Siddique, N., Fecto, F., Chen, W., Yang, Y., Liu, E., Donkervoort, S., Zheng, J.G., Shi, Y., Ahmeti, K.B., Brooks, B., Engel, W.K., Siddique, T., 2010. Frameshift and novel mutations in FUS in familial amyotrophic lateral sclerosis and ALS/dementia. Neurology 75, 807–814. http://dx.doi.org/10.1212/WNL.0b013e3181f07e0c.
Yu, D.X., Di Giorgio, F.P., Yao, J., Marchetto, M.C., Brennand, K., Wright, R., Mei, A., Mchenry, L., Lisuk, D., Grasmick, J.M., Silberman, P., Silberman, G., Jappelli, R., Gage, F.H., 2014. Modeling hippocampal neurogenesis using human pluripotent stem cells. Stem Cell Rep. 2, 295–310. http://dx.doi.org/10.1016/j.stemcr.2014.01.009.